Biphasic, Switch-Like Isothermal DNA Amplification

Burcu Özay‡, Cara M Robertus‡, Jackson L Negri, and Stephanie E McCalla*

‡ Authors contributed equally to this manuscript

Department of Chemical and Biological Engineering, Montana State University, Bozeman, MT, 59717, USA

ABSTRACT: Switch-like reactions are common in the natural world; they are vital to basic cellular operations such as signaling and genetic regulation. Synthetic systems have aimed to reproduce this effect for applications from DNA computing to molecular diagnostics. These systems can produce switch-like behavior, but typically respond to nanomolar input of target molecule. We report a novel DNA amplification chemistry that has two switch-like characteristics. First, the chemistry is biphasic, with a low-gain initial phase and plateau followed by a high gain burst of signal. Second, the reaction kinetics can produce a large ultrasensitive jump in signal during the second phase. Reaction output at each stage can be rationally tuned based on DNA association thermodynamics. The chemistry is one-step, isothermal, and can be adapted to respond to a broad range of input target molecules. This isothermal DNA amplification reaction could potentially impact a variety of disciplines such as synthetic biology, biosensors, DNA computing, and clinical diagnostics.

Switch-like responses to input stimuli are ubiquitous in nature. This switching behavior is common in cell signaling, transcription, and genetic regulatory networks; it is commonly accepted that these switches react decisively to a true signal while filtering out noise[1]. These biological switches typically have two defining characteristics: the first is a definitive "on" and "off" state, and the second is a large ultrasensitive jump in output when above a threshold input. Ultrasensitivity can stem from a variety of mechanisms[2] such as molecular titration[3], sponging[4], multistep signaling[5], homo-multimerization[6], zero-order ultrasensitivity[7], or cooperativity[8,9]. Researchers are using these mechanisms to create biomimetic switches, as they have noted the utility of ultrasensitive amplification kinetics in biosensors, genetic logic gates, DNA circuits, and materials that are required to be highly responsive[10-12].

Several studies have reported switch-like behavior in synthetic biochemical systems. Ion channels can be repurposed into biosensor switches by preventing channel dimerization in the presence of an target antigen, thus turning on in the presence of target[13]. DNA oscillators can switch between an "on" and "off" state by combining DNA degradation with a DNA amplification reaction[14]. The authors noted that the oscillatory effect could be achieved through non-linear DNA amplification instead of non-linear DNA degradation, but the former is currently difficult to obtain and manipulate. Structure-switching sensors such as aptamers[15] and molecular beacons[16,17] change conformation in the presence of a specific target molecule. When properly designed, structure-switching biosensors can also create Hill-type ultrasensitive kinetics: biosensors with two cooperative binding sites produce an ultrasensitive response if the affinity of the target for the second site is altered by target association to the first site[11,12,18]. These exciting biomimetic systems can stably produce simple, digital (yes/no) outputs with nanomolar trigger inputs, but they have not yet been designed for low input target concentrations. A single cell can contain as few as 10 microRNA molecules per cell[19], and clinically relevant DNA and RNA concentrations range from hundreds of picomolars to attomolar in range[20]. Clinically relevant protein concentrations are often in the femtomolar range[21]. While previous studies explored sensors that turn on and off with ultrasensitive Hill-type kinetics or created controlled switches, they do not have the subsequent high-gain amplification required for low target concentrations.

We present a simple, tunable nucleic acid amplification method with an endogenous switching mechanism. The method exploits a naturally occurring stall in the amplification reaction, which produces a low-level signal. Upon surpassing a threshold, the reaction enters a high-gain second phase "burst", producing a signal that ranges from ten to one hundred times the base DNA amplification reaction. We hypothesize that cooperative opening of a stable looped DNA template creates the high-gain burst. Output kinetics can be tuned to create an ultrasensitive jump that resembles a definitive switch turn-on. The reaction is isothermal and rapid, with a sub-picomolar limit of detection for input trigger DNA. These oligonucleotide triggers can be produced from proteins[22-26], genomic bacterial DNA[27], viral DNA[28], microRNA[29], or mRNA[30], making this technique applicable to a broad range of biological sensors.

EXPERIMENTAL SECTION

Reagents. UltraPure™ Tris-HCI pH 8.0, RNase free EDTA, RNase free $MgCl_2$, RNase free KCl, Novex™ TBE Running Buffer (5X), 2X TBE-Urea Sample Buffer, Novex™ TBE-Urea Gels, 15%, SYBR® Gold Nucleic Acid Gel Stain, and SYBR® Green II RNA Gel Stain were purchased from Thermo Fisher Scientific (Waltham, MA). Nuclease-free water and oligo length standard 10/60 were purchased from Integrated DNA Technologies, Inc. (Coralville, IA). Nt.BstNBI nicking endonuclease, Bst 2.0 WarmStart® DNA Polymerase, 10x ThermoPol I Buffer, dNTPs, BSA, and 100 mM $MgSO_4$ were purchased from New England Biolabs (Beverly, MA).

Oligonucleotides were ordered from two different sources to avoid trigger contamination in templates. Desalted amplification templates were purchased from Integrated DNA Technologies (Coralville, IA) suspended in IDTE Buffer at a concentration of 100 µM. Templates were modified with an amino group on the 3' end to prevent template extension. All desalted trigger oligonucleotides were purchased from Eurofins Genomics (Louisville, KY) suspended at a concentration of 50 µM in TE Buffer. Triggers were diluted in nuclease-free water in a separate room to prevent contamination.

Template design and thermodynamics. Thermodynamics of the template stem loops were determined using the Mfold web server[31], an open source software that uses empirical free energies of DNA hybridization[32] that have been corrected for salt concentration[33] (http://unafold.rna.albany.edu/?q=mfold). The free energies of association between the template and trigger, template and elongated trigger, product dimers, and double stranded templates were determined using the DINAmelt application, two-state melting (http://unafold.rna.albany.edu/?q=DINAMelt/Two-state-melting). To determine the free energy of toehold association, the software input was the sequence of the toehold and the toehold reverse compliment. All settings used were kept at the default software parameters, except for temperature (55°C) and salt concentration ($[Na^+]$ = 60mM, $[Mg^{++}]$ = 6mM).

Biphasic Amplification Reactions. The amplification reaction mixture contained 1x ThermoPol I Buffer [20 mM Tris-HCl (pH 8.8), 10 mM $(NH_4)_2SO_4$, 10 mM KCl, 2 mM $MgSO_4$, 0.1% Triton® X-100], 25 mM Tris-HCl (pH 8), 6 mM $MgSO_4$, 50 mM KCl, 0.5 mM each dNTP, 0.1 mg/mL BSA, 0.2 U/µL Nt.BstNBI, and 0.0267 U/µL Bst 2.0 WarmStart® DNA Polymerase. Bst 2.0 WarmStart® DNA polymerase is inactive below 45°C; this decreases non-specific amplification before reaction initiation and theoretically increases experimental reproducibility. Templates were diluted in nuclease-free water and added at a final concentration of 100 nM. SYBR Green II (10,000x stock in DMSO) was added to the reaction mixture to a final concentration of 5x. Reactions were prepared at 4°C, and triggers and templates were handled in separate hoods to prevent contamination. Triggers were diluted in nuclease-free water and added to positive samples to a final concentration of 10 pM unless otherwise indicated; negative controls contained no trigger. For each experiment, two controls were prepared: a no-template control (NTC) sample containing no template, and a no-enzyme control sample containing no enzymes. Reactions were run in triplicate 20 µL volumes. Fluorescence readings were measured using a Bio-Rad CFX Connect Thermocycler (Hercules, CA). Measurements were taken every 20 seconds with a 12 second imaging step. Reactions were run for either 150 or 300 cycles of 32 seconds at 55°C. The mixture was heated to 80°C for 20 minutes to deactivate enzymes, followed by 10°C for five minutes to cool the samples. Completed reactions were stored at -20°C for further analysis.

Product quantification. NanoDrop 3300 Fluorospectrometer (Thermo Scientific, Wilmington, DE) was used for measuring the reaction product concentrations. The standards (ssDNA oligos, Eurofins Genomics, Louisville, KY) and the reaction products were diluted in 1X TE buffer (1mM Tris-HCl, 0.5 mM EDTA) if needed. Nucleic acid stains were diluted in 1X TE Buffer. 1X SYBR® Gold Nucleic Acid Gel Stain (for low concentration samples) or 2.5X SYBR® Green II RNA Gel Stain (for high concentration samples), and 1.2 µL of the sample were brought to a final volume of 12 µL with 1X TE buffer. The standards were prepared in the same way as the reaction products with the addition of mock reaction product (reaction components without enzymes or trigger) and triggers diluted in 1X TE Buffer. Samples were excited with blue light (470 ± 10 nm) with autogain on. The fluorescence peaks of the dyes were determined to be 512 nm for SYBR® Green II RNA Gel Stain and 536 nm for SYBR® Gold Nucleic Acid Gel Stain for the specific salt conditions, and the average fluorescence of 5 replicate measurements was used to determine the product concentrations of the reaction products. 1X TE buffer was used as the blank measurement.

Data analysis. Real-time reaction traces were analyzed with custom software using Matlab (Natick, MA). Details on calculation of inflection points, plateaus, and reaction rates can be found in the SI (Figure SI 4, custom matlab analysis software). The ratios between maximum reaction rates, plateaus, and inflection points were calculated from two experiments with three experimental replicates each. When appropriate, data from two experiments were averaged using a weighted average[34]. Spearman's rank-order correlations and p-values were determined using the function "corr" with the type selected as "Spearman" in Matlab (Natick, MA). Further details of statistical analysis can be found in the SI under "statistics".

RESULTS AND DISCUSSION

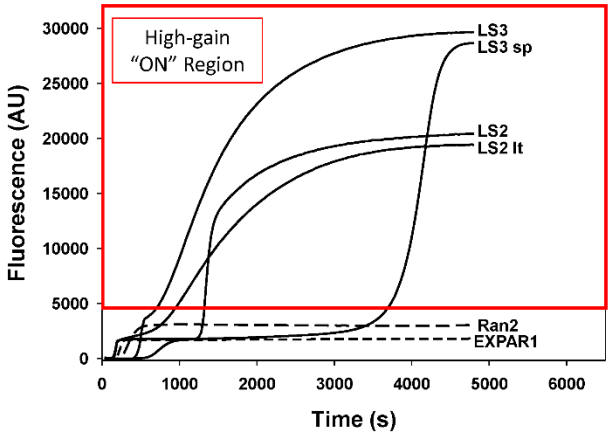

FIGURE 1 Representative biphasic amplification reaction output. DNA amplification output is correlated to fluorescence, which increases and plateaus at approximately the same level as previously reported optimized EXPAR reactions[35,36]. Biphasic DNA amplification output is shown in solid lines, with previously reported EXPAR amplification output shown in dotted lines. After a lag period, the DNA output jumps into a high gain "on" region with tunable kinetics. Template DNA names are labeled next to corresponding output traces; template sequences can be found in the Table SI 1.

Reaction pathways in the biphasic DNA amplification reaction. The biphasic DNA amplification reaction contains the same base components as the exponential amplification reaction for oligonucleotides (EXPAR)[37]. Both EXPAR and the biphasic DNA amplification reaction amplify a trigger sequence of ten to twenty base pairs in length at a single reaction temperature of 55°C through the action of a thermophilic polymerase and a nicking endonuclease. Both reactions will non-

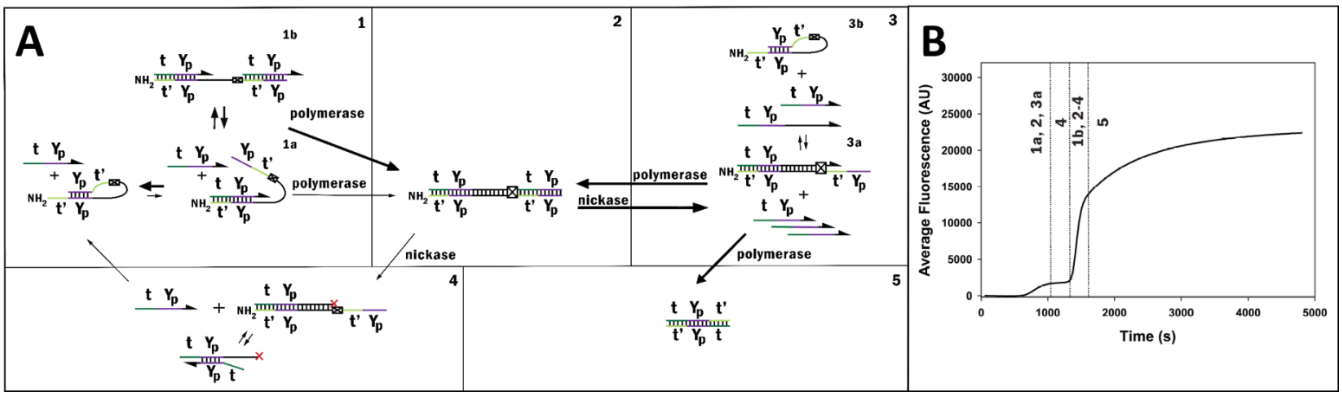

FIGURE 2 Biphasic DNA amplification reaction. (A) The cartoon depicts potential reaction pathways in the biphasic DNA amplification reaction. The amplification requires a looped DNA template with two palindromic sequences (Yp), two toeholds (t'), and a restriction site (⊠), as well as polymerase and nickase enzymes. The reaction amplifies a DNA trigger with a reverse compliment to the template toehold (t) and the palindromic region (Yp); arrows show extendable 3' ends of the DNA. The trigger can bind to either toehold region t' and strand displace the palindromic region Yp, thus opening the loop (1). A polymerase can then extend the trigger and create the recognition site for a nicking endonuclease (2), as well as an identical trigger. The nickase then cuts the top strand (3a), freeing the newly created trigger to bind other templates (1). The loop can also remove the long trigger and close with the aid of short triggers, which can bind the long trigger and facilitate loop closure (3b, 4). This may be vital to remove "poisoned" long triggers that cannot amplify and block further trigger amplification on the template (4). The palindromic region can also cause trigger dimerization, after which the toehold regions can be filled by the polymerase; this removes trigger molecules from further amplification cycles (5). (B) A representative reaction trace of template LS2; the reaction stages are labeled with proposed reaction mechanisms that govern each stage.

specifically create product in the absence of initial DNA trigger. The main difference between the original EXPAR reaction and the biphasic oligonucleotide amplification reaction is the palindromic sequence within the DNA template that causes the template to fold into a looped configuration. The thermodynamics of the trigger binding and DNA association are in a regime that creates a biphasic DNA amplification reaction; EXPAR-type DNA amplification using looped templates are found in literature[38-40], but the biphasic ultrasensitive kinetics have not yet been reported.

Representative outputs of the oligonucleotide amplification reaction are shown in Figure 1. Despite the similarities in reaction components, the biphasic amplification reaction reported here is functionally distinct from all other EXPAR reactions. The first phase of the reaction resembles traditional EXPAR output, with an initial rise and a first plateau. Thermodynamics of the looped DNA template and trigger association are well correlated with the first-phase reaction kinetics (Spearman's R = 0.8022, Figure SI 1) when compared to the original EXPAR reaction (R = 0.4072)[35]. This is likely due to the closed template loop; thermodynamics of DNA association dominate the reaction kinetics, contrasting the sequence dependence seen in traditional EXPAR. After the first plateau, the biphasic reaction enters a high-gain second phase. This finding reveals that EXPAR can recover from the first plateau, a fact that was previously unknown. The one template that favors a linear configuration at the reaction temperature (LS3 lowpG2, T_m = 49.2^{0}C) gives biphasic output, implying that while a palindromic region is necessary for biphasic output, a stable loop structure is not.

The mechanism behind the switch-like oligonucleotide amplification reaction is likely driven by multiple phenomena, as shown in Figure 2A. The DNA template is composed of two copies of the complementary sequence joined by a nine nucleotide nicking enzyme recognition site, specifically containing: a 3' amine group to prevent extension of the template, a 3' toehold, a palindromic sequence, the nickase recognition site, the repeated 5' toehold, and the repeated palindromic sequence (panel 1). The palindromic region causes the template to fold into a looped configuration. Triggers for these templates consist of the toehold complement and the template palindrome. When a trigger binds to the 3' end of the template, the DNA polymerase extends the strand and the nicking enzyme recognition site is created (panel 2). The nickase then nicks the growing strand (panel 3a). The polymerase extends at this nick and displaces the downstream trigger (panel 3a → 2). The displaced trigger is then free to prime other templates, leading to exponential amplification (panel 3a → 1). The amplification therefore produces both triggers and long triggers that contain the nickase recognition site on their 3' end (panel 3b). The presence of the palindromic sequence produces several new reaction pathways. The palindromic section of the triggers can associate, be extended by the polymerase, and create inert triggers unable to further replicate; this pathway has been previously discussed[38] (panel 5). The trigger can catalyze removal of the long, stable trigger by binding to either the palindromic region of the long trigger or by binding to the template (panel 3b, 4). Loop closure will also aid in removal of trigger and long trigger from the template. Finally, the presence of the loop with two toehold regions creates cooperative binding between the triggers and the looped template. For most templates, the looped configuration is more stable than the open, trigger-bound configuration (Table SI 2). The association of the template and the first trigger molecule will open the loop, which both aids and stabilizes a second trigger association (panel 1b). We hypothesize that these new reaction pathways create the unique features of our amplification reaction detailed in Figure 2B.

Properties of the first reaction phase. The first reaction phase resembles the base EXPAR reaction, with a rapid, low-gain reaction phase followed by a plateau. While this stall was previously attributed to loss of nickase integrity, the recovery of the reaction after the first plateau invalidates this theory. Recently others have hypothesized that some templates could

be "poisoned" due to polymerase errors that render the DNA strand bound to the template unextendible (Figure 2a, panel 5)[41]. We hypothesize that this could cause the plateau seen in the original EXPAR reaction and the first plateau in the biphasic amplification reaction (Figure 2B). We estimated the plateau trigger concentration to be on the order of 1 µM (Figure SI 2), which ten times greater than the template concentration. Due to the rapid template inactivation after ten cycles of extension and nicking it is unlikely that polymerase error causes this plateau, given error rates of polymerases such as *Bst* DNA polymerase that lack the $3' \rightarrow 5'$ exonuclease domain are approximately 10^{-4} [42]. We hypothesize that the plateau is due to noncanonical behavior of the nickase enzyme that leaves a long unextendible trigger (Figure 2a panel 4), as the nickase is operating in suboptimal conditions when compared to the polymerase[36]. It is also possible that a fully elongated trigger poisons the template; the mechanism behind the template poisoning is beyond the scope of this study.

Properties of the second reaction phase. After the first plateau, the amplification enters a high-gain second phase followed by a second plateau. The amplification does not exit the first plateau unless there is a palindromic region in the template; we hypothesize that template rescue is aided by trigger association to the long "poisoned" triggers (Figure 2A, panel 4). This trigger-dependent rescue would prevent the long trigger from reassociating with the template, particularly after polymerase extension of the 3' trigger end. The trigger could also dynamically bind the template and prevent reassociation of the long trigger. These events would aid in the loop closure and template rescue. After exiting the first plateau many of the templates exhibit Hill-like second phase kinetics, marked by a large jump in reaction product that greatly exceeds first phase reaction kinetics. We hypothesize that this ultrasensitivity is caused by homotropic allosteric cooperativity; the trigger can bind either toehold as seen in Figure 1 panel 1. The template loop structure is stable when compared to the trigger:template association (Table SI 2), and the accumulation of reaction products would shift templates to an open, amplification competent state and produce nonlinear reaction kinetics $\left({}^{d([trigger])}/_{dt} \propto [trigger]^2\right)$.

The subsequent second plateau is caused by exhaustion of reaction components and a buildup of inhibitory reaction byproducts. This effect of inhibitory products was previously described when using EXPAR reactions and a palindromic looped template[38]. The final output of the second phase is approximately the size of the DNA triggers as seen in PAGE analysis of reaction products; for more details see the Supplementary Information (Figure SI 3). This rescue of the poisoned templates allows the reaction to produce 10-100 times more endpoint reaction product as measured by calibrated SYBR II fluorescence. Endpoint product concentration ranged from 7.8 – 116.9 µM, with several reaction products exceeding 100 µM during the second plateau (Table SI 3).

Reaction response to initial trigger concentration. We measured reaction output in real-time with varying initial trigger concentrations using the ssDNA binding dye SYBR II for fluorescent readout. Figure 3A shows the average of three real-time fluorescent traces with varying initial trigger concentrations normalized to the fluorescence at the second inflection point. The first and second inflection points correspond to the times at which maximum first derivative of the fluorescence occur for the first and second reaction phase (Figure SI 4).

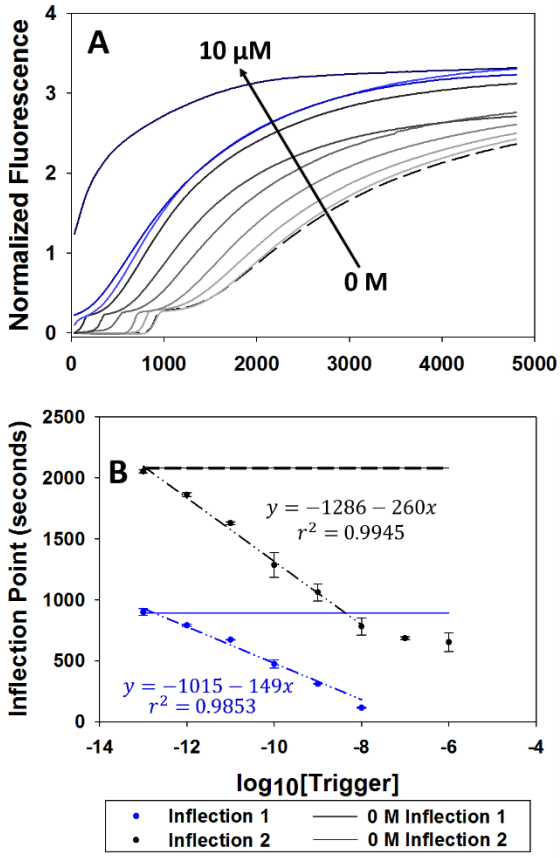

FIGURE 3 Correlation between onset of amplification and trigger oligonucleotide concentration. (A) The real-time reaction output for a representative template LS3 lrs-4 shows the dependence of the reaction on initial trigger concentration, with fluorescence correlated to the produced DNA trigger. Triggers concentrations were increased tenfold between 100 fM and 10 µM. Blue traces did not have measurable first reaction phases; high concentrations of trigger (≥1 µM) bypass the first reaction phase entirely, implying that the plateau of this template is on the order of [trigger] = 1 µM. (B) The inflection points are experimental triplicates, and the dotted lines are linear fits. The solid lines show inflection point of the negative control (0 M initial trigger concentration), with surrounding dashed lines showing the standard deviation of the negative control inflection point (not visible for the second inflection point, ± 1.8 s). The first inflection points vary linearly with the log of initial trigger concentration, and the second inflection points vary linearly with the log of initial trigger concentration when initial trigger concentration is ≤ 10 nM. Error bars represent standard deviation of experimental triplicates.

Inflection points are traditionally used as a surrogate for EXPAR reaction kinetics. The first reaction phase was not present for high trigger concentrations ≥ 1 µM, which was the approximate concentration of reaction products quantified during the plateau phase of a biphasic amplification reaction (Figure SI 2). High concentrations of trigger appeared to prevent the reaction from entering the plateau phase, which suggested that entering the second reaction phase is dependent on trigger concentration or rate of trigger production. The inflection points of the first phase are linearly correlated to the log of the initial trigger concentration, which is also true of EXPAR reactions[36] (Figure 3B). The second phase inflection

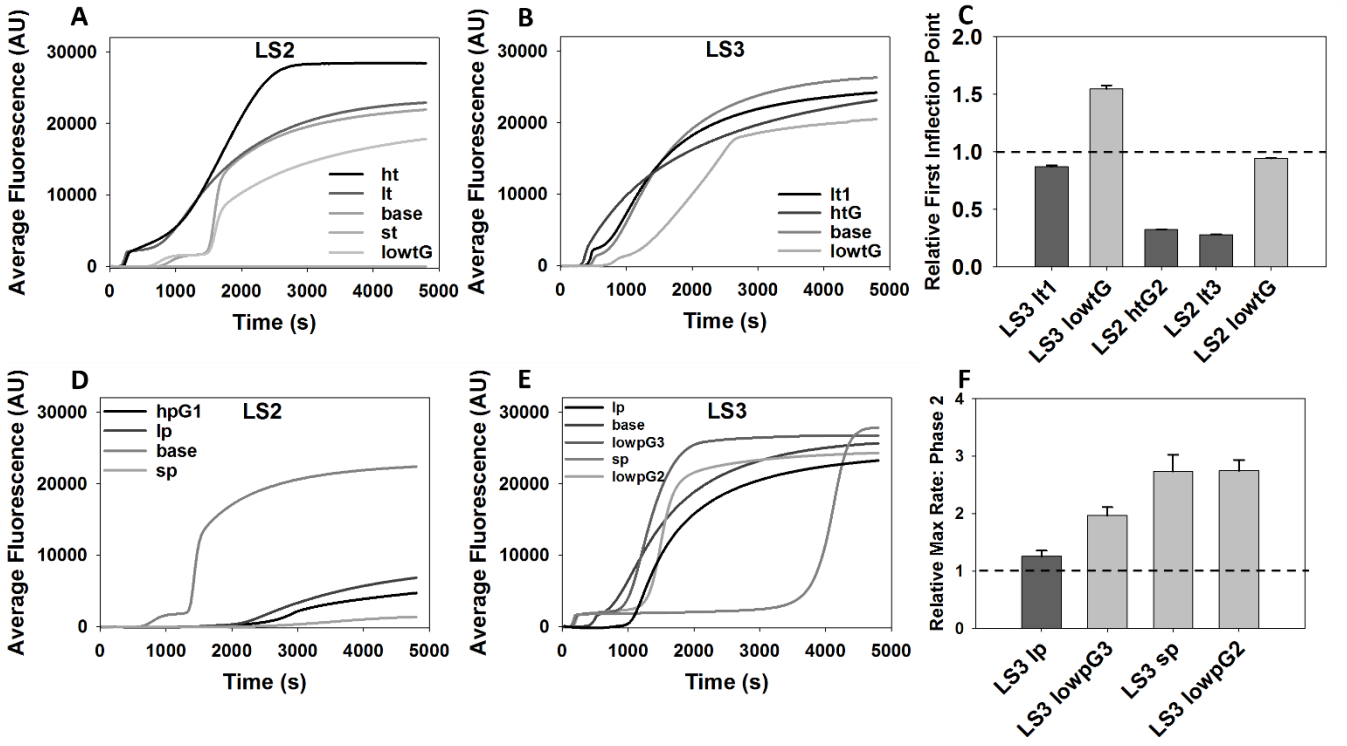

FIGURE 4: Effect of toehold and palindrome free energy on template performance. (A) Amplification curves of LS2 toehold variants, with the strongest toeholds in black and weaker toeholds in lighter shades of grey. (B) Amplification curves of LS3 toehold variants, with stronger toeholds in black and weaker toeholds in lighter shades of grey. (C) The templates shown in the bar graph are in order from strongest to weakest toehold free energies with respect to the base template (LS2 or LS3). Darker bars have stronger toeholds than the base templates, lighter bars have weaker toeholds than the base template, and the dotted lines show an inflection point equal to the base template. The relative first inflection point is the time of the first inflection point divided by the first inflection point of the base templates LS2 or LS3. D) Amplification curves of LS2 palindrome variants, with the strongest palindrome in black and weaker palindromes in lighter shades of grey. (E) Amplification curves of LS3 palindrome variants. (F) The templates shown in the bar graph are in order from strongest to weakest palindrome free energies, with darker grey signifying the templates with stronger palindromes than the base template. The relative maximum second phase reaction rate is the maximum slope (dF/dt) in the second rise divided by the maximum dF/dt in the second rise of the base template (LS3), which is a relative measure of the second phase reaction kinetics.

points also linearly correlated with the log of the initial trigger concentration for low initial concentrations of trigger (≤ 10 nM). As with traditional EXPAR, the limit of detection for the DNA trigger was determined by the nonspecific amplification rates; the reaction in Figure 3 has a sub-picomolar limit of detection, and nearly all templates reported here could distinguish between 0 and 10 pM initial trigger concentrations (Figure SI 5).

Varying toehold thermodynamics within templates. We varied toehold thermodynamics of two base template designs LS2 and LS3, and examined the relative contributions of toehold strength to reaction output. Toehold thermodynamics varied both by modifying the length or GC content of the template and trigger toehold region. For both template LS2 (Figure 4A) and template LS3 (Figure 4B), increasing the length of the toehold generally causes the loop to open more rapidly, thus lowering the first phase inflection point. LS2 lowtG had a lower GC content and slightly faster first phase kinetics than LS2, which deviated from the expected trend (Figure 4C). This deviation may be caused by competing reaction mechanisms, such as a weaker long trigger and rapid recovery of poisoned template (Figure 2A, box 4). Template LS2 st also fell outside the expected trend; although it did not have the weakest toehold, it failed to produce measurable amounts of trigger (Figure 4A). This was likely due to the small trigger size; at 8 nucleotides, polymerization or nicking may have been inefficient.

Varying palindrome thermodynamics within templates. We varied the thermodynamics of the palindromic template and trigger region by modifying the length or the GC content of the palindrome. Increasing the strength of the palindrome for template LS2 decreased the ability of the trigger to open the stable template stem-loop structure (Figure 4D). This resulted in a slower reaction with subtle biphasic responses, making these templates ineffective as molecular switches. Reaction kinetics slowed dramatically when the free energy of the palindrome is lowered by replacing original palindrome base pairs with GC pairs (LS2 hpG1) or lengthening the palindrome (LS2 lp). Although decreasing the palindrome length favored trigger binding and subsequent loop opening, shortening the palindrome slowed the reaction kinetics. This is likely because template LS2sp was also unusually short and paired with an 8 nucleotide trigger, which may again have caused polymerization or nicking kinetics to be inefficient. All LS2 variant templates demonstrated altered kinetics, and their almost negligible first phases were difficult to accurately quantify.

Figure 4D & E demonstrates the effects of changing palindrome strength for the base template LS3. Decreasing the free

energy of the palindrome caused the plateau phase to increase in length and the maximum reaction rate to increase in magnitude. Conversely, increasing the free energy of the palindrome nearly eliminates the first phase. It is possible that this behavior is caused by the strong palindromic region of the trigger binding to the long "poisoned" trigger-template and subsequent loop closure; this would facilitate template rescue as shown in Figure 2A (panel 4).

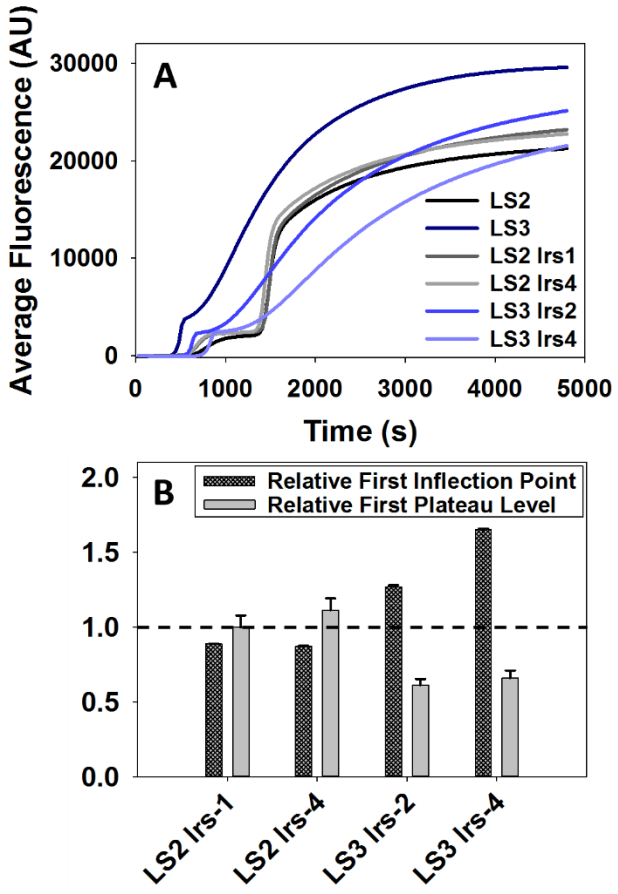

FIGURE 5: Varying the loop strength of looped templates. (A) Amplification curves of LS2 and LS3 loop variants, with the strongest loops for LS2 in black and the strongest loops for LS3 in dark blue. Weaker loops are indicated by lighter shades of grey or blue. (B) The templates shown in the bar graph are in order from strongest to weakest loop free energies with respect to the base template (LS2 and LS3). All lrs templates have weaker loop structures when compared to the base templates.

Varying loop thermodynamics within templates. Figure 5 demonstrates another important source of kinetic variability: the strength of the loop. The free energy of the looped template structure was altered by adding long random sequences into the loop before the recognition site, which held the palindrome, toehold, and trigger sequences constant while varying stability of the template stem-loop structure. The only additional thermodynamic parameter this changed was an increase in stability of the long trigger:template complex. For template LS2, decreasing the strength of the loop caused the loop to open faster, thereby decreasing the first inflection point as expected. This alteration did not have a large effect on the height of the first plateau. Surprisingly, decreasing the strength of the LS3 template loop slowed the first reaction phase (Figure 5B). We hypothesize that this phenomenon was caused by the increased stability of the long triggers, which included the original trigger sequence, the restriction site, and the long random sequences. These long triggers were more stable and more difficult to remove, which may have caused the lower relative product concentration at the reaction plateau seen in Figure 5B. Trigger binding to the long inactive trigger and loop closure that rescue the template (Figure 2A, panel 4) appear to control the height and duration of the first plateau. LS3 templates had greater loop stability, greater trigger:template stability, and stronger toeholds when compared to the LS2 family of templates. It is possible that templates LS2 and LS3 operate in different reaction regimes with distinct dominant reaction pathways. Due to the many contributing reaction mechanisms, the effect of loop thermodynamics was not consistent between template families.

Analyzing the ultrasensitive response of the second reaction phase. We further analyzed DNA amplification kinetics for their Hill-like behavior to determine if ultrasensitive kinetics in the second phase correlated with DNA association thermodynamics. We approximate Hill-type behavior using the ratio of the maximum reaction rate in the second phase to the maximum reaction rate in the first phase. A larger ratio would correspond with more pronounced Hill-type behavior, as the reaction would receive a large kinetic boost at higher trigger concentrations building in the second phase (see Figure SI 4 for details of this calculation). Using thermodynamic parameters of DNA association, we analyzed the hypothesis that two trigger binding sites on the amplification template caused Hill-type kinetics by homotropic cooperativity.

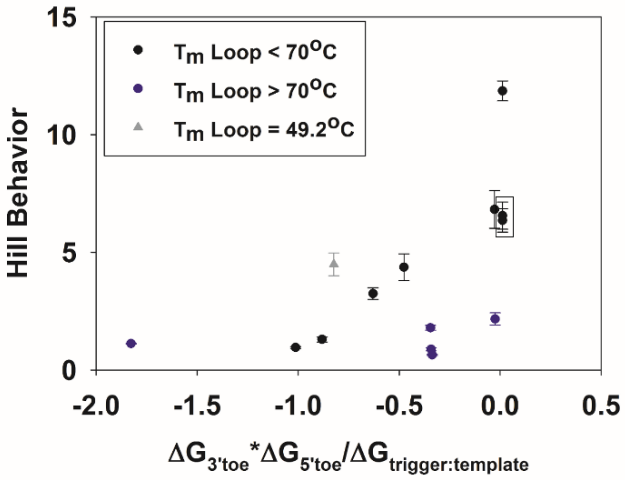

FIGURE 6: Cooperativity and ultrasensitivity of second phase kinetics. If the cooperativity of trigger binding to the two open toeholds contributed to Hill-type kinetics, then the parameter $T = \Delta G_{5'toehold} * \Delta G_{3'toehold} / \Delta G_{trigger:template}$ would correlate with Hill-type behavior. A correlation is seen in all templates that are stable at the reaction temperature and have a melting temperature < 70°C (Spearman R = 0.8783, p < 0.01), but not seen for the most stable loops with melting temperatures > 70°C.

Hill coefficients of a homotropic cooperative receptor increase with the ratio between dissociation constants of the first and second binding events; a large difference in stability between the first and second ligand associations will result in a larger Hill coefficient and greater Hill behaviour[12]. This is qualitatively intuitive: the more relative stability that the first association provides, the greater the benefit from having a higher concentration of ligand. In our system, this corre-

sponds to the amplification incompetent state (a closed template) moving to an amplification competent state (an open template) through dual trigger binding. We characterized the relative dissociation of the first and second trigger binding events by the parameter: $T = \Delta G_{5',toehold} * \Delta G_{3',toehold} / \Delta G_{trigger:template}$, with a less negative value signifying a greater difference between the stability of the first and second trigger associations to the template. While this parameter does not fully incorporate loop strength for templates with a long random sequence added (boxed in Figure 6), it approximates the relative dissociation when one and two trigger molecules are bound to the template. There is a strong correlation between T and Hill behavior for templates that have a stable loop structure at 55°C but a melting temperature <70°C from both the LS2 and LS3 families (Figure 6, Spearman R = 0.8783, $p < 0.01$). This correlation supported the hypothesis that toehold cooperativity contributed to ultrasensitive kinetics in the second phase for these templates. The association of one trigger with these templates was thermodynamically unfavorable when compared to the stable loop structure (Table SI 2), but upon association the trigger will open the loop structure and switch the receptor to a binding competent state (Figure 2A, panel 1). Templates in the LS3 family with Tm > 70°C again deviate from the expected trend; all have minimal acceleration in the late phase, minimal Hill behavior, and do not correlate with the parameter T (Spearman R = 0.1). Interestingly, these templates show greater acceleration in the second phase with more favorable template rescue, which is not seen in templates with Tm < 70°C. (Spearman R = -1, $p < 0.02$, Figure SI 7).

CONCLUSIONS

DNA association thermodynamics roughly correlate with the main reaction features: first phase reaction kinetics, first plateau, and second phase reaction kinetics. The strength of the toehold and trigger association with the template both correlate with kinetics in the first phase, suggesting that the probability of opening the stable looped template structure will largely determine the first phase output. The ability of the template and triggers to remove long triggers appears to be a secondary factor in determining the first phase kinetics. We hypothesize that the accumulation of "poisoned" templates with bound unextendible long triggers may slow the reaction, which occur approximately once per every ten trigger extensions. These "poison" long triggers also appear to affect the plateau level: strongly bound long triggers will freeze the reaction faster than weakly bound long triggers, lowering the trigger concentration seen at the plateau.

Second phase kinetics are more complex. Templates with a strong loop structure did not show Hill-type acceleration in the second phase. It is possible that these template populations never favor the open, binding competent structure over the closed loop structure at the existing trigger concentrations. With a thermodynamically favorable loop and palindrome binding region, it is possible that the long trigger removal and loop closure shown in panel 3b and 4 is a dominant reaction pathway. This is supported by the correlation between thermodynamics of long trigger removal and reaction acceleration in the second phase. Templates with a loop melting temperature below 70^0C show faster kinetics in the second phase when toeholds are thermodynamically weaker when compared to association of the full trigger, suggesting homotropic cooperativity. When the template melts below the reaction temperature, these correlations no longer apply but the reaction remains biphasic. These observations provide important design considerations to tune the reaction output during each phase.

Future applications of this biphasic DNA amplification reaction require further investigation and optimization. Due to multiple contributing reaction pathways, the relationship between DNA association thermodynamics and reaction output is currently defined by approximate correlations. Reaction design would be aided by mathematical modeling of reaction kinetics and a full mechanistic understanding of the reaction phases. As with many isothermal amplifications such as EXPAR, this reaction also produces non-specific amplification occurring at long reaction times in the absence of an oligonucleotide trigger. Non-specific amplification will increase the limit of detection and can decrease the experimental robustness. Adding ssDNA binding proteins and carbon sheets[43] or other small molecules[44] can decrease non-specific amplification in EXPAR reactions, and would likely also be applicable in this reaction. Degradation of the reaction product was previously used to create a bistable switch from an EXPAR-type reaction[14], and could be extended to suppress non-specific amplification or create threshold-based detection for targets above a chosen concentration. Inhibition or degradation of reaction products could also create a true bistable switch that could repeatedly turn "off" and "on" with tunable ultrasensitive kinetics.

We have demonstrated a novel new biosensor with a two-stage output based on the concentration of a released trigger molecule. The biphasic DNA amplification reaction is a simple, one-step isothermal amplification reaction; reactions of this type have gained popularity as they do not require temperature cycling and therefore require less energy, hardware, and time[45,46]. We have described a general reaction design framework to rationally tune first phase kinetics and second phase ultrasensitive DNA output. This chemistry can be tuned by changing the thermodynamics of the looped template and reporter DNA molecules. In the future, we will expand the capabilities of the reaction: trigger DNA oligonucleotides can be created by proteins[22-26], genomic bacterial DNA[27], viral DNA[28], microRNA[29], or mRNA[30], making the biphasic DNA amplification reaction broadly applicable to a variety of target molecules. When combined with digital (single molecule) amplification, this technique has the potential to be quantitative. The biphasic nature of this reaction makes it well suited for recognition of low-concentration molecules in biological samples, DNA logic gates, and other molecular recognition systems.

ASSOCIATED CONTENT

Supporting Information

The Supporting Information is available free of charge on the ACS Publications website.

List of templates and triggers, DNA binding thermodynamics, list of final product concentrations, measured product concentrations during the reaction, correlation between template thermodynamics and first inflection point, PAGE gel images and analysis, graphical description of kinetic parameters used, details of data analysis and statistics, and separation time between positive and negative control reactions (PDF).

AUTHOR INFORMATION

Corresponding Author

* Email: stephanie.mccalla@montana.edu

Author Contributions

The manuscript was written through contributions of all authors, and all authors have given approval to the final version of the manuscript. ‡BÖ and CMR contributed equally.

ACKNOWLEDGMENT

This publication was supported by the National Center For Advancing Translational Sciences of the National Institutes of Health [UL1 TR002319] and the Montana Research and Economic Development Seed Funds.

REFERENCES

(1) Ferrell, J. E. *Trends in biochemical sciences* **1996**, *21*, 460-466.
(2) Zhang, Q.; Bhattacharya, S.; Andersen, M. E. *Open biology* **2013**, *3*, 130031.
(3) Buchler, N. E.; Louis, M. *Journal of molecular biology* **2008**, *384*, 1106-1119.
(4) Mukherji, S.; Ebert, M. S.; Zheng, G. X.; Tsang, J. S.; Sharp, P. A.; van Oudenaarden, A. *Nature genetics* **2011**, *43*, 854-859.
(5) Huang, C.-Y.; Ferrell, J. E. *Proceedings of the National Academy of Sciences* **1996**, *93*, 10078-10083.
(6) Notides, A. C.; Lerner, N.; Hamilton, D. E. *Proceedings of the National Academy of Sciences* **1981**, *78*, 4926-4930.
(7) Meinke, M. H.; Bishop, J. S.; Edstrom, R. D. *Proceedings of the National Academy of Sciences* **1986**, *83*, 2865-2868.
(8) Ha, S.; Ferrell, J. *Science* **2016**, *352*, 990-993.
(9) Adair, G. S. *Journal of Biological Chemistry* **1925**, *63*, 529-545.
(10) Plaxco, K. W.; Soh, H. T. *Trends in Biotechnology*, *29*, 1-5.
(11) Simon, A. J.; Vallée-Bélisle, A.; Ricci, F.; Plaxco, K. W. *Proceedings of the National Academy of Sciences* **2014**, *111*, 15048-15053.
(12) Simon, A. J.; Vallée-Bélisle, A.; Ricci, F.; Watkins, H. M.; Plaxco, K. W. *Angewandte Chemie* **2014**, *126*, 9625-9629.
(13) Cornell, B. A.; Braach-Maksvytis, V.; King, L.; Osman, P. *Nature* **1997**, *387*, 580.
(14) Montagne, K.; Gines, G.; Fujii, T.; Rondelez, Y. *Nature Communications* **2016**, *7*, 13474.
(15) Zuo, X.; Song, S.; Zhang, J.; Pan, D.; Wang, L.; Fan, C. *Journal of the American Chemical Society* **2007**, *129*, 1042-1043.
(16) Vallée-Bélisle, A.; Ricci, F.; Plaxco, K. W. *Proceedings of the National Academy of Sciences* **2009**, *106*, 13802-13807.
(17) Tyagi, S.; Kramer, F. R. *Nature biotechnology* **1996**, 303-308.
(18) Ricci, F.; Vallée-Bélisle, A.; Simon, A. J.; Porchetta, A.; Plaxco, K. W. *Accounts of Chemical Research* **2016**, *49*, 1884-1892.
(19) Zhou, Y.; Huang, Q.; Gao, J.; Lu, J.; Shen, X.; Fan, C. *Nucleic acids research* **2010**, *38*, e156-e156.
(20) Kelley, S. O. *ACS Sensors* **2017**, *2*, 193-197.
(21) Rissin, D. M.; Kan, C. W.; Campbell, T. G.; Howes, S. C.; Fournier, D. R.; Song, L.; Piech, T.; Patel, P. P.; Chang, L.; Rivnak, A. J. *Nature biotechnology* **2010**, *28*, 595-599.
(22) Zhang, Z.-z.; Zhang, C.-y. *Analytical Chemistry* **2012**, *84*, 1623-1629.
(23) Tang, W.; Zhang, T.; Li, Q.; Wang, H.; Wang, H.; Li, Z. *RSC Advances* **2016**, *6*, 89888-89894.
(24) Qiu, T.; Wang, Y.; Yu, J.; Liu, S.; Wang, H.; Guo, Y.; Huang, J. *RSC Advances* **2016**, *6*, 62031-62037.
(25) Nutiu, R.; Li, Y. *Journal of the American Chemical Society* **2003**, *125*, 4771-4778.
(26) Wieland, M.; Benz, A.; Haar, J.; Halder, K.; Hartig, J. S. *Chemical Communications* **2010**, *46*, 1866-1868.
(27) Roskos, K.; Hickerson, A. I.; Lu, H.-W.; Ferguson, T. M.; Shinde, D. N.; Klaue, Y.; Niemz, A. *PLoS ONE* **2013**, *8*, e69355.
(28) Tan, E.; Erwin, B.; Dames, S.; Voelkerding, K.; Niemz, A. *Clinical chemistry* **2007**, *53*, 2017-2020.
(29) Zhang, X.; Liu, C.; Sun, L.; Duan, X.; Li, Z. *Chemical Science* **2015**, *6*, 6213-6218.
(30) Zhao, Y.; Zhou, L.; Tang, Z. *Nat Commun* **2013**, *4*, 1493.
(31) Zuker, M. *Nucleic acids research* **2003**, *31*, 3406-3415.
(32) SantaLucia, J. *Proceedings of the National Academy of Sciences* **1998**, *95*, 1460-1465.
(33) Peyret, N. *Prediction of nucleic acid hybridization: parameters and algorithms*; Wayne State University Detroit, 2000.
(34) Taylor, J. *Introduction to error analysis, the study of uncertainties in physical measurements*, 1997.
(35) Qian, J.; Ferguson, T. M.; Shinde, D. N.; Ramírez-Borrero, A. J.; Hintze, A.; Adami, C.; Niemz, A. *Nucleic acids research* **2012**, *40*, e87-e87.
(36) Tan, E.; Erwin, B.; Dames, S.; Ferguson, T.; Buechel, M.; Irvine, B.; Voelkerding, K.; Niemz, A. *Biochemistry* **2008**, *47*, 9987-9999.
(37) Van Ness, J.; Van Ness, L. K.; Galas, D. J. *Proceedings of the National Academy of Sciences* **2003**, *100*, 4504-4509.
(38) Fujii, T.; Rondelez, Y. *ACS nano* **2012**, *7*, 27-34.
(39) Padirac, A.; Fujii, T.; Estévez-Torres, A.; Rondelez, Y. *Journal of the American Chemical Society* **2013**, *135*, 14586-14592.
(40) Zambrano, A.; Zadorin, A. S.; Rondelez, Y.; Estévez-Torres, A.; Galas, J. C. *The Journal of Physical Chemistry B* **2015**, *119*, 5349-5355.
(41) Baccouche, A.; Montagne, K.; Padirac, A.; Fujii, T.; Rondelez, Y. *Methods* **2014**, *67*, 234-249.
(42) Lage, J. M.; Leamon, J. H.; Pejovic, T.; Hamann, S.; Lacey, M.; Dillon, D.; Segraves, R.; Vossbrinck, B.; González, A.; Pinkel, D. *Genome Research* **2003**, *13*, 294-307.
(43) Wang, J.; Zou, B.; Rui, J.; Song, Q.; Kajiyama, T.; Kambara, H.; Zhou, G. *Microchimica Acta* **2015**, *182*, 1095-1101.
(44) Mok, E.; Wee, E.; Wang, Y.; Trau, M. *Scientific reports* **2016**, *6*.
(45) McCalla, S. E.; Tripathi, A. *Annual review of biomedical engineering* **2011**, *13*, 321-343.
(46) Li, J.; Macdonald, J. *Biosensors and Bioelectronics* **2015**, *64*, 196-211.